NUKLEONIKA 2013;58(1):203–206

ORIGINAL PAPER

# Uniqueness of studies on electron densities in the extended momentum space

**Grażyna Kontrym-Sznajd**

**Abstract.** This work draws attention to the fact that by measuring electronic structure via angular correlation of positron radiation (ACAR) and Compton scattering experiments one probes electron densities in the extended momentum space, directly related to the electron Bloch wave functions. Presenting some examples of electron densities in the extended and reduced momentum spaces, it is demonstrated what kind of information concerning the electronic structure can be obtained depending on the considered space. It is also shown how the knowledge of the symmetry selection rules allows to separate various Fermi surfaces and establish Fermi momenta.

**Key words:** electron-positron momentum densities • Compton scattering • extended momentum space • positron annihilation

G. Kontrym-Sznajd
W. Trzebiatowski Institute of Low Temperature and Structure Research, Polish Academy of Sciences, 2 Okólna Str., P. O. Box 1410, 50-950 Wrocław 2, Poland, Tel.: +48 71 395 4131, Fax: +48 71 344 1029, E-mail: g.sznajd@int.pan.wroc.pl

Received: 14 June 2012
Accepted: 11 October 2012

The Fermi surface (FS), related to many material properties such as transport, optical and equilibrium properties, is also responsible for some exotic phenomena. Experimentally, it can be studied by techniques based on periodic oscillations of various physical quantities in a magnetic field [27] and "non-magnetic" methods as Compton scattering [6], angular correlation of annihilation radiation (ACAR) [5], and angle-resolved photoemission spectroscopy (ARPES) [7]. Whereas magnetic methods (as e.g. dHvA effect) allow to estimate only some quantities related to FS (e.g. area of extremal electron orbits or an effective mass), ACAR, ARPES or Compton scattering spectra (measured at arbitrary temperatures and often also in magnetic field [26, 32]) yield information on the shape of FS in the whole reciprocal space [8, 15].

ACAR and Compton scattering experiments probe an electron density $\rho(\mathbf{p})$ in the extended $\mathbf{p}$-space

$$\rho(\mathbf{p}) = \sum_j n_{\mathbf{k}j} \left| \int_{-\infty}^{\infty} e^{-i\mathbf{p}\cdot\mathbf{r}} \psi_{\mathbf{k}j}(\mathbf{r}) d\mathbf{r} \right|^2 \tag{1}$$

which contains information not only on the occupied momentum states (and hence FS) but also on the Umklapp components (see Fig. 1) of the electron wave functions $\psi_{\mathbf{k}j}(\mathbf{r})$ in the state $\mathbf{k}$ of $j$-th band. The main difference between these two experiments consists in the fact that in the Compton scattering plane projections of electron momentum densities are measured while in the case of ACAR spectra, the electron-positron (e-p) momentum densities, $\rho^{e\text{-}p}(\mathbf{p})$ ($\psi_{\mathbf{k}j}(\mathbf{r})$ in Eq. (1) represents e-p wave functions), either via plane or line projections (one-dimensional, 1-D, or two-dimensional, 2-D, spectra). By measuring spectra along different

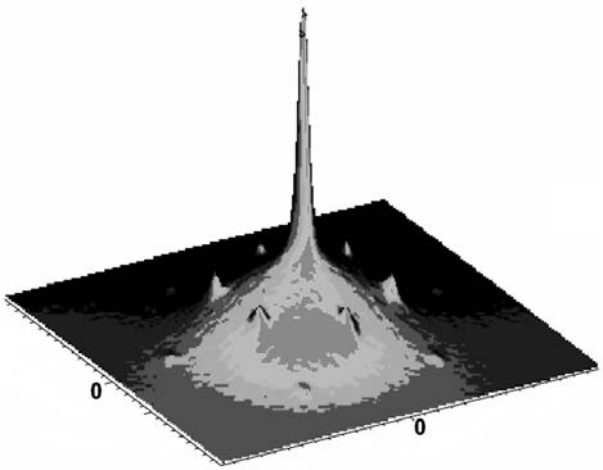


**Fig. 1.** 2-D ACAR experimental spectrum for the hexagonal α-quartz in the momentum range – 2 up to 2 atomic units of momentum. It represents integration of a density $\rho^{e\text{-}p}(\mathbf{p})$, containing both central peak and Umklapp components, along directions parallel to the hexagonal c-axis (more details in [15]).

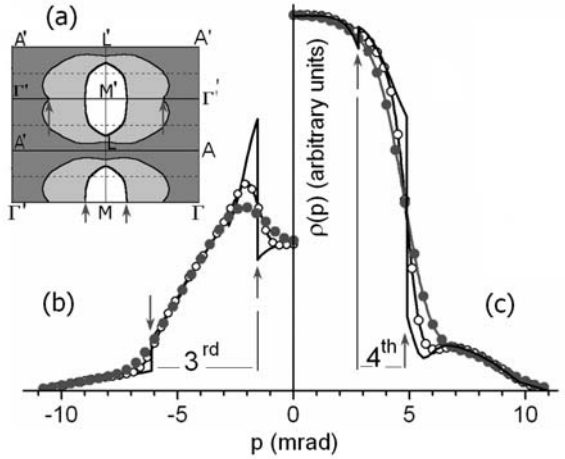


**Fig. 2.** Theoretical Fermi surface in Y on the ΓMLA plane (part (a)), in the repeated zone scheme, derived from Loucks [21]. Electrons in the 3rd and 4th zones are marked by grey and white colours, respectively. Theoretical densities $\rho(\mathbf{p})$ along ΓM on the first basal plane and along Γ'M' on the parallel plane are drawn by the solid line in the parts (c) and (b), respectively. Fermi momenta $\mathbf{p}_F$ for the 3rd and 4th bands are marked by arrows. Lines with full and open circles show the theoretical $\rho(\mathbf{p})$ after smearing by two Gaussians, simulating the raw and deconvoluted experimental data.

directions, 3-D (three-dimensional) densities $\rho(\mathbf{p})$, directly related to the electron Bloch wave function, can be reconstructed from experiment [15].

Taking into account the complexity of a many-body problem of electrons and a positron moving within a lattice potential, almost all interpretations of experimental ACAR data are performed only from the point of view of the FS studies. In order to obtain the contour of FS, the best way is to fold $\rho(\mathbf{p})$ from the extended zone $\mathbf{p}$ into the reduced momentum space via the LCW (Lock, Crisp, West) folding [20] getting

$$\rho(\mathbf{k}) = \sum_{\mathbf{G}} \rho(\mathbf{p} = \mathbf{k} + \mathbf{G}) = \sum_{j} f_j(\mathbf{k}) n_j(\mathbf{k}) \tag{2}$$

where $\mathbf{k}$ denotes vectors in the first Brillouin zone, $\mathbf{G}$ means the reciprocal lattice vector, $n_j = \{1,0\}$ is the occupation number modified by a function $f_j(\mathbf{k})$ which contains both many-body and positron wave function effects (in the case of Compton scattering $f_j(\mathbf{k}) = 1$).

However, due to the finite resolution of an equipment, it can happen that there is no possibility to separate from $\rho(\mathbf{k})$ some FS sheets when they are close one to another. In the $\mathbf{p}$ space, they are separated in a natural way because their contribution appears for different reciprocal lattice vectors $\mathbf{G}$ (so-called symmetry selection rules [11]). Such situation takes place, e.g. in yttrium, where $\mathbf{k}$ space analysis of the densities reconstructed from 2-D ACAR data [10] allowed to get the shape and size of the so-called webbing FS, though without separating their elements in the 3rd and the 4th zones. Further interpretation of the same data but in terms of $\rho(\mathbf{p})$ allowed to separate these two FSs and to determine some Fermi momenta $\mathbf{p}_F$ [17].

Almost all theoretical calculations of electronic structure of trivalent hcp (hexagonal close packing) yttrium, e.g. [21, 24] and references in [17]) deliver the same FS topology: the first two bands are fully occupied and the FS exists in the 3rd and 4th bands. The 3rd valence band does not contribute to $\rho(\mathbf{p} = \mathbf{k} + \mathbf{G})$ for $\mathbf{G} = (000)$, (i.e. along ΓM) but it does for $\mathbf{G} = (001)$ (along Γ'M') while the 4th band has a dominant contribution on the first basal ΓMK plane. Due to such properties of $\rho(\mathbf{p})$, it was possible to separate these two FS by drawing a zero contour of differences between the deconvoluted and raw densities, similarly as in Fig. 5 in Ref. [10]. Such a way of finding $\mathbf{p}_F$ (explained in Fig. 1 in Ref. [9]) is demonstrated here in Fig. 2 by the intersection of two lines which simulate raw (lines with open circles) and deconvoluted (lines with full circles) experimental data. As it is seen, this method works very well in the case of the 4th band (Fig. 2c). Unfortunately, it is not the case when densities have such shape as shown in the part (b), i.e. after crossing the FS $\rho(\mathbf{p})$ is rapidly decreasing. However, making such tests for theoretical densities as shown in Fig. 2 (smearing them by a few Gaussian distributions) one can estimate corrections which should be introduced in order to determine $\mathbf{p}_F$ from experimental densities.

A similar situation took place in $LaB_6$ [16]. Only from $\rho(\mathbf{p})$ (reconstructed from 2-D ACAR data) in the extended zone it was possible to derive a small electron pocket in the 15th band along ΓM line (see white square ΓXMX in Fig. 3), not seen earlier by the analysis of the

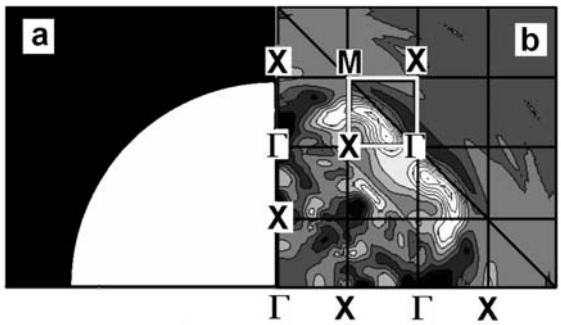


**Fig. 3.** Densities in the extended $\mathbf{p}$ space on the plane (001) in $LaB_6$ reconstructed from 2-D ACAR spectra: a – free--electron sphere containing 27 electrons with the radius of the momentum 1.18 a.u.; b – anisotropic part of the reconstructed $\rho(\mathbf{p})$ [16]. They are shown with the Brillouin zone boundaries drawn in the repeated zone scheme.

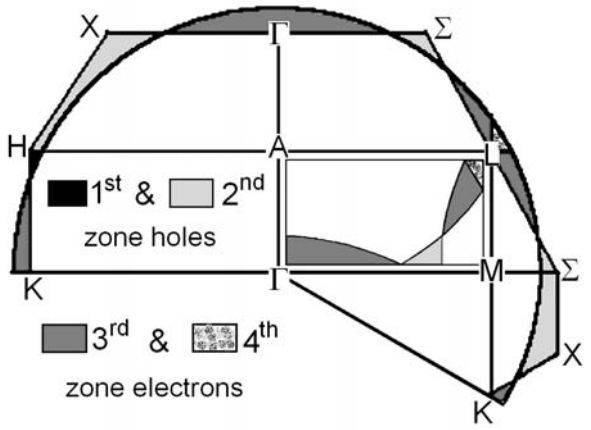


**Fig. 4.** Free-electron FS of divalent hcp metal in the extended **p** space with marked (inside the plane ΓMLA) FS elements in the reduced **k** space.

same 2-D ACAR data in the **k** space [3]. This pocket, observed in dHvA experiments [23, 29, 30], also appear in the latest band structure results [12]. Moreover, the isotropic average of reconstructed densities $\rho_0(p)$, forms a sphere whose volume equals 13.5 volumes of the Brillouin zone that contains 27 valence electrons. Sometimes such information concerning the number of valence electrons, available only in the **p** space, is very important.

The next physical phenomena that should be studied in the extended zone are many-body effects [1, 2, 4, 14, 25, 28]. Of course, they can be studied in the reduced zone, as it has been proposed lately in Ref. [19], but their understanding is possible only in the **p** space because they are connected with wave functions what is discussed in detail in Ref. [18]. Moreover, as shown by Šob [31], even in such simple metals as alkalis, in particular in Rb and Cs, the contribution of Umklapp components is relatively high (up to 25%). Since some theories of the e-p interactions give similar behaviour of densities inside the central FS but differ completely in the Umklapp region [28], these facts constitute a basis for further theoretical investigations of e-p interaction in solids, however, in the **p** space.

It is also clear that a reconstruction of 3-D densities from their projections should be carried out in the extended zone, although it was also applied to experimental projections brought to the zone **k** [22]. It can be simply illustrated by the example of free-electron FS of divalent hcp metal (i.e. containing 2 electrons/atom what in the case of hcp structure corresponds to 4 electrons/unit cell), displayed in Fig. 4.

When reconstruction is performed in the **p** space, for fully isotropic densities only one projection is needed. Otherwise, after conversion from **p** into **k** space, the corresponding spherical FS consists of the following elements: the 1st zone holes around H, the 2nd zone holes (so-called monster), 3rd zone electrons around: L (butterflies), Γ (lens), K (called either needles or cigars), and the 4th zone electron pockets around L. So, the reconstruction of such a complex FS where $\rho(\mathbf{k})$ is changing from 0 (holes in the first zone) up to 4 (electrons in the 4th zone) needs a lot of projections. Therefore, as the first step the reconstruction of $\rho(\mathbf{p})$ is needed and then performing LCW folding, if it is necessary.

## Summarizing

A purpose of this work is to draw attention to the fact that electron momentum densities in the extended momentum space, so directly related to wave functions, can be obtained by performing ACAR and Compton scattering experiments. This allows to study not only the FS but also Umklapp components or, e.g. orbital character of dopants, studied lately with high-resolution Compton scattering in a cuprate superconductor [13] or many body correlation effects. Such unique information cannot be obtained using other techniques of the FS studies as well as without analysis of experimental ACAR or Compton scattering data in the extended **p** zone.

## References

1. Alatalo M, Barbiellini B, Hakala M *et al*. (1996) Theoretical and experimental study of positron annihilation with core electrons in solids. Phys Rev B 54:2397–2409
2. Arponen J, Pajanne E (1979) Angular correlation in positron annihilation. J Phys F: Metal Phys 9:2359–2376
3. Biasini M, Fretwell HM, Dugdale SB *et al*. (1997) Positron annihilation study of the electronic structure of $LaB_6$ and $CeB_6$. Phys Rev B 56:10192–10199
4. Boronski E, Szotek Z, Stachowiak H (1981) Exact solution of the Kahana equation for a positron in an electron gas. Phys Rev B 23:1785–1795
5. Brandt WA, Dupasquier A (eds) (1983) Positron solid-state physics. North-Holland Publishing, Amsterdam
6. Cooper MJ, Mijnarends PE, Shiotani N, Sakai N, Bansil A (eds) (2004) X-ray Compton scattering. Oxford University Press, Oxford
7. Damascelli A, Hussain Z, Shen Z-X (2003) Angle-resolved photoemission studies of the cuprate superconductors. Rev Mod Phys 75:473–541
8. Dugdale SB (2007) Exploring and mapping Fermi surfaces of complex materials. Phys Status Solidi C 4:3851–3856
9. Dugdale SB, Alam MA, Fretwell HM, Biasini M, Wilson D (1994) Application of maximum entropy technique to extract Fermi surface topology from positron annihilation measurements. J Phys: Condens Matter 6:L435–L443
10. Dugdale SB, Fretwell HM, Alam MA, Kontrym-Sznajd G, West RN, Badrzadeh S (1997) Direct observation and calipering of the webbing Fermi surface of yttrium. Phys Rev Lett 79:941–944
11. Harthoorn R, Mijnarends PE (1978) The effect of symmetry on electron momentum distributions in solids. J Phys F: Metal Phys 8:1147–1158
12. Hossain FM, Riley DP, Murch GE (2005) "Ab initio" calculations of the electronic structure and bonding characteristics of $LaB_6$. Phys Rev B 72:235101–235106
13. Hughes ID, Däne M, Ernst A *et al*. (2007) Lanthanide contraction and magnetism in the heavy rare earth elements. Nature 446:650–653
14. Kahana S (1963) Positron annihilation in metals. Phys Rev 129:1622–1628
15. Kontrym-Sznajd G (2009) Fermiology via the electron momentum distribution (review article). Fizika Nizkikh Temperatur 35:765–778 (Low Temp Phys 35:599–609)
16. Kontrym-Sznajd G, Samsel-Czekała M, Biasini M, Kubo Y (2004) Band structure of $LaB_6$ by an algorithm for filtering reconstructed electron-positron momentum densities. Phys Rev B 70:125103 (10 pp)
17. Kontrym-Sznajd G, Samsel-Czekała M, Pietraszko A *et al*. (2002) Electron momentum density in yttrium. Phys Rev B 66:155110 (10 pp)

18. Kontrym-Sznajd G, Sormann H, Boroński E (2012) General properties of electron-positron momentum densities. Phys Rev B 85:245104 (9 pp)
19. Laverock J, Haynes TD, Alam MA, Dugdale SB (2010) Experimental determination of the state-dependent enhancement of the electron-positron momentum density in solids. Phys Rev B 82:125127 (13 pp)
20. Lock DG, Crisp VHC, West RN (1972) Positron annihilation and Fermi surface studies: a new approach. J Phys F: Metal Phys 3:561–570
21. Loucks TL (1966) Fermi surface and positron annihilation in yttrium. Phys Rev 144:504–511
22. Manuel AA (1982) Construction of the Fermi surface from positron-annihilation measurements. Phys Rev Lett 49:1525–1528
23. Matsui H, Goto T, Kunii S, Sakatsume S (1993) Acoustic de Haas-van Alphen effect in $LaB_6$ and $CeB_6$. Physica B 186/188:126–128
24. Matsumoto M, Staunton JB, Strange P (1991) Relativistic spin-polarised "ab initio" calculations of the anisotropy and temperature dependence of the paramagnetic spin susceptibility of scandium and yttrium. J Phys: Condens Matter 3:1453–1460
25. Rubaszek A, Szotek Z, Temmerman WM (2002) Understanding electron-positron momentum densities in paramagnetic chromium. Phys Rev B 65:125104 (5 pp)
26. Sakurai H, Ota M, Itoh F, Itou M, Sakurai Y, Koizumi A (2006) Anisotropies of magnetic Compton profiles in Co/Pd multilayer system. Appl Phys Lett 88:062507
27. Shoenberg D (1984) Magnetic oscillations in metals. Cambridge University Press, Cambridge
28. Sormann H (1996) Influence of lattice effects on the electron-positron interaction in metals. Phys Rev B 54:4558–4580
29. Suzuki T, Goto T, Fujimura T, Kunii S, Suzuki T, Kasuya T (1985) Acoustic de Haas-van Alphen effect and rotational invariance of $LaB_6$. J Magn Magn Mater 52:261–263
30. Suzuki T, Goto T, Ohe Y, Fujimura T, Kunii S (1988) Novel technique of acoustic de Haas van Alphen effect and application to $LaB_6$. J Phys C 8:799–800
31. Šob M (1985) Electron momentum density and the momentum density of positron annihilation pairs in alkali metals: high-momentum components. J Phys F: Metal Phys 15:1685–1691
32. Żukowski E, Andrejczuk A, Dobrzyński L *et al*. (2000) Spin-dependent electron momentum density in $Fe_3Si$ and $Fe_3Al$. J Phys: Condens Matter 12:7229–7241